HHS Public Access

Author manuscript

Exp Eye Res. Author manuscript; available in PMC 2021 July 01.

Published in final edited form as:

Exp Eye Res. 2020 July ; 196: 108064. doi:10.1016/j.exer.2020.108064.

Segmental Differences Found in Aqueous Angiographic-Determined High- and Low-Flow Regions of Human Trabecular Meshwork

Sindhu Saraswathy[1], **Thania Bogarin**[1], **Ernesto Barron**[1], **Brian A. Francis**[1], **James C.H. Tan**[1], **Robert N. Weinreb**[2], **Alex S. Huang**[1]

[1)]Doheny Eye Institute and Department of Ophthalmology, David Geffen School of Medicine at UCLA, Los Angeles, CA, USA

[2)]Hamilton Glaucoma Center, Shiley Eye Institute, and the Viterbi Family Department of Ophthalmology University of California, San Diego, CA, USA

Abstract

This work sought to compare aqueous angiographic segmental patterns with bead-based methods which directly visualize segmental trabecular meshwork (TM) tracer trapping. Additionally, segmental protein expression differences between aqueous angiographic-derived low- and high-outflow human TM regions were evaluated. Post-mortem human eyes (One Legacy and San Diego eye banks; n = 15) were perfused with fluorescent tracers (fluorescein [2.5%], indocyanine green [0.4%], and/or fluorescent microspheres). After angiographic imaging (Spectralis HRA+OCT; Heidelberg Engineering), peri-limbal low- and high-angiographic flow regions were marked. Aqueous angiographic segmental outflow patterns were similar to fluorescent microsphere TM trapping segmental patterns. TM was dissected from low- and high-flow areas and processed for immunofluorescence or Western blot and compared. Versican expression was relatively elevated in low-flow regions while MMP3 and collagen VI were relatively elevated in high-flow regions. TGF-β2, thrombospondin-1, TGF-β receptor1, and TGF-β downstream proteins such as α-smooth muscle actin were relatively elevated in low-flow regions. Additionally, fibronectin (FN) levels were unchanged, but the EDA isoform (FN-EDA) that is associated with fibrosis was relatively elevated in low-flow regions. These results show that segmental aqueous angiographic patterns are reflective of underlying TM molecular characteristics and demonstrate increased pro-fibrotic activation in low-flow regions. Thus, we provide evidence that aqueous angiography outflow visualization, the only tracer outflow imaging method available to clinicians, is in part representative of TM biology.

Corresponding Author: Alex Huang, MD/PhD, Doheny Eye Institute, Department of Ophthalmology, David Geffen School of Medicine, University of California, Los Angeles, 1355 San Pablo Street, Los Angeles, CA 90033, Ahuang@Doheny.org, Phone: 323-342-6436; Fax: 323-342-6688.

Keywords

Glaucoma; Segmental Aqueous Humor Outflow; Aqueous angiography; Trabecular Meshwork; Outflow Imaging

Introduction

Glaucoma is a leading cause of irreversible vision loss with elevated intraocular pressure (IOP) as the most important risk factor (Weinreb and Khaw, 2004). In the normal eye, IOP is maintained by a balance between aqueous humor production and its outflow (Brubaker, 2004). Aqueous humor outflow (AHO) occurs through two routes, the conventional and the unconventional pathways (Johnson, 2006). The majority of AHO moves through the conventional pathway, and here a major source of outflow resistance is the trabecular meshwork (TM) (Abu-Hassan et al., 2014; Swaminathan et al., 2014). Due to an impairment or dysfunction in these drainage pathways, there is increased outflow resistance in many forms of glaucoma which leads to increased IOP and risk for optic neuropathy (Johnson, 2006; Morrison et al., 2011).

More than treating the outflow pathways as one-unit, recent investigation has also shown that AHO is segmental and not circumferential nor uniform around the limbus (Carreon et al., 2017; Cha et al., 2016; Chang et al., 2014; Huang et al., 2017c; Huang et al., 2018; Huang et al., 2016a; Huang et al., 2016b; Sabanay et al., 2000; Saraswathy et al., 2016). Different limbal regions show segmental high- or low-AHO. Structural assessments using optical coherence tomography (OCT) (Huang et al., 2017a) or computed tomography (3D-CT) (Hann et al., 2011) have shown segmental AHO physical characteristics. To identify where aqueous flows, microbead tracers were added to human anterior segment perfusion culture which showed segmental uptake in the TM (Vranka et al., 2015; Vranka et al., 2018). Linking segmental flow to structural features, outflow pathways near higher-flow regions have shown more collector channels (Bentley et al., 2016). In higher flow regions, Schlemm's canal (SC) cells have more border-pores which are conduits for aqueous (Braakman et al., 2014; Braakman et al., 2015; Gong et al., 2002; Tamm, 2009).

However, the molecular basis for segmental AHO flow is not fully elucidated. Previously, tracer-based studies have identified and isolated high- and low-flow TM (Carreon et al., 2017; Chang et al., 2014; Keller et al., 2011; Vranka et al., 2015). There were elevated levels of versican RNA and protein (a large proteoglycan) in low flow regions of human anterior segment culture TM (Keller et al., 2011). Then, using microarrays and immunolabeling, a variety of extracellular matrix (ECM) and ECM-relevant transcripts and proteins were found to be differentially expressed in high- and low-flow TM regions (Vranka and Acott, 2017; Vranka et al., 2015). Matrix metalloproteinases (MMP 1, 2, and 3) as well as collagen gene transcription such as collagen VI were enriched in the high-flow regions (Vranka et al., 2015) at physiologic pressures. TM immunostaining specifically confirmed that the MMP3 and collagen type VI (COLVI) alternations are at a protein level (Vranka et al., 2015). Quantitative proteomic analyses of segmental low- and high-flow TM regions showed heavy representation of ECM proteins as well as ECM differences comparing areas of different

flow before and after exposure to elevated intraocular pressure (Vranka et al., 2018) Elevated COLVI was now seen in low-flow regions at higher pressures (Vranka et al., 2018).

Our recent work introduced aqueous angiography as an additional method to visualize AHO. Aqueous angiography delivers fluorescent tracers into the anterior chamber followed by external angiographic imaging of the ocular surface (Saraswathy et al., 2016). With this technique, the intrascleral venous plexus and more distal aqueous and episcleral veins have been visualized. Aqueous angiography has been performed in multiple species in enucleated whole globes (porcine, bovine, feline, and human), and all show segmental AHO (Huang et al., 2016a; Snyder et al., 2019). In living organisms, aqueous angiography continued to show segmental AHO in non-human primates and humans in the operating room (Huang et al., 2017c) (Huang et al., 2017b). Additional observations were that AHO was pulsatile, dynamic, and capable of improvement. In enucleated human whole globes and glaucoma patient eyes, trabecular bypass rescued low-flow regions (Huang et al., 2019; Huang et al., 2016b). Thus, aqueous angiography supported the idea of segmental AHO in both enucleated post-mortem eyes and in living subjects. However, since aqueous angiography only visualizes distal outflow, questions persist as to how reflective it is of outflow at the level of the TM.

In the present study, we used aqueous angiography to visualize segmental distal AHO patterns to isolate high- and low-flow TM from post-mortem human eyes. This was done for two purposes. Like prior investigation of high- and low-flow TM, we sought to identify molecular differences between these two regions to better understand segmental AHO. Also, since aqueous angiography is the only method that can assess AHO in live humans using tracers, another purpose was to compare molecular segmental differences in the TM (obtained based upon aqueous angiographic guidance) to published results based upon other bead-based methods using anterior segment perfusion culture which directly visualize the TM. By showing that aqueous angiography-determined TM shows similar patterns of known segmental proteins, clinicians can have further confidence that clinical aqueous angiography-based patterns seen on the ocular surface reflect underlying TM biology and molecular differences.

2. Methods

2.1. Aqueous Angiography

Post-mortem human eyes (n = 15) (One Legacy Eye Bank, Los Angeles, CA; San Diego Eye Bank, San Diego, CA; or Saving Sight Eye Bank, Kansas City, MO) were obtained within 48 hours of death (Supplemental Table 1). The 15 eyes came from 11 donors. None of the protein comparison experiments directly compared two eyes from the same donor. Eyes with a history of glaucoma noted on eye bank provided medical history were excluded. Eyes were oriented by inferior oblique insertion location/orientation and pinned to Styrofoam. A Lewicky anterior chamber (AC) maintainer (BVI Visitec; Alcester, UK) was inserted inferiorly through a 1-mm side port (Alcon; Fort Worth, TX) into the anterior chamber and perfused with Balanced Salt Solution (BSS; Alcon) for one hour at a pressure of ~10 mm Hg based on gravity (Camras et al., 2012). Eyes were kept moist with room temperature (RT) BSS-soaked gauze.

Aqueous angiography was performed as described before (Huang et al., 2016a; Huang et al., 2016b; Saraswathy et al., 2016). Fluorescein (25%; Akorn; Lake Forest, IL) was diluted at RT in BSS to 2.5%. Indocyanine green (ICG, I2533; Sigma, St. Louis, MO) dissolved with water into a 2% stock solution that was subsequently diluted in BSS to 0.4%. For studies using fluorescent microspheres (0.2pm, F8764, FITC-labeled, Thermo Fisher Scientific, CA), they were diluted (1:500) into BSS or 0.4% ICG and vortexed vigorously. The eyes were placed in front of the Spectralis HRA+OCT (Heidelberg Engineering; Heidelberg, Germany; **fluorescein capture mode**: excitation wavelength= 486 nm and transmission filter set at > 500 nm; **ICG capture mode**: excitation wavelength= 786 nm and transmission filter set at > 800 nm) with fluorescent images taken using a 55-degree lens at a 25-diopter focus. Confocal scanning laser ophthalmoscopic (cSLO) infrared images were taken to center the eye. Prior to tracer application, cSLO fluorescent angiographic images using the fluorescein or ICG capture mode were taken to provide a standard pre-tracer intensity background image which appeared black. Then, aqueous humor was exchanged with the tracer that had a reservoir height set for ~10 mm Hg. High- and low-flow regions were marked with a surgical marking pen on the peripheral cornea. These marks were readily visible so that they served as reference points during TM removal or creation of wedges for sectioning after opening the eyes, as described below.

2.2. Immunofluorescence

For immunofluorescence studies, six post-mortem human eyes were used. After aqueous angiography (three each perfused with ICG or fluorescein), the eyes were perfused and fixed with 4% paraformaldehyde for 15 minutes at 10 mm Hg. Wedges including the angle were cut from angiographically positive and negative regions and then placed in 4% PFA for an additional 15 minutes. Five micron-thick paraffin sections were cut onto Superfrost Plus slides, air dried, and de-paraffinized. Sections were blocked in 5% bovine serum albumin (BSA), permeabilized with 0.3%Triton X-100, and subjected to immunofluorescent labelling using specific primary antibodies against versican (Abcam [Cambridge, UK]: ab19345, polyclonal 1:100), MMP3 (Antibody Verify [Las Vegas, NV]: AAS41420C, polyclonal 1:100), α-smooth muscle actin (αSMA) (Sigma: A5228, monoclonal 1:100), fibronectin-EDA (Accurate Chemical and Scientific Corp. [Westbury, NY]: YM7092, monoclonal 1:100), fibronectin (Abcam: ab2413, polyclonal 1:100), COL-VI (Developmental Studies Hybridoma Bank [Iowa City, IA]: SC6, monoclonal 1:100), TSP-1 (Abcam: Ab 85762, polyclonal 1:100) and species specific secondary antibodies (Thermo-Fisher Scientific [Waltham, MA], Texas Red anti-mouse or anti-rabbit, 1:100). Negative controls included conditions which lacked primary antibody but included secondary antibodies only. Slides were then mounted with a 4’,6-diamidino-2-phenylindole (DAPI)-containing mounting medium and viewed under a Keyence BZX700 digital imaging microscope (Keyence; Chicago, IL). Sections were imaged using a 4x plan-fluor lens with a 0.13 numerical aperture. All images were taken using identical settings for illumination and image capture sensitivity (Keyence imaging software v.1.51). For Texas Red (EX BP 560/40, DM 585, EM BP 630/75) and DAPI (EX BP 360/40, DM 400, EM BP 460/50) appropriate filters were used respectively.

2.3. Western Blot

For Western blot analyses a total of five eyes were used. After ICG aqueous angiography, peri-limbal high- and low-angiographic signal regions were marked with a surgical marker. Each eye was then dissected, and TM near high- and low-signal angiographic regions was dissected using a stereomicroscope with careful attention to avoid iris or other contaminating tissues. TM corresponding to each region type (high- or low-angiographic signal) were pooled for each eye as they were often found in non-contiguous segments. Each eye served as one sample, and comparisons were performed in triplicates. Total protein was extracted by homogenizing the tissue in protein extraction buffer (RIPA Buffer; Thermo-Fisher Scientific) containing protease inhibitors cocktail (Sigma, P8340, 1:100) followed by centrifugation at ~16,000g for 25 minutes (4°C). Protein quantification of the supernatant was determined using a Bradford assay (Bio-Rad Laboratories; Hercules, CA) with BSA as the standard. Samples were denatured and reduced with 2-mercaptoethanol (Bio-Rad, Hercules, CA) and Laemmli buffer (Bio-Rad Laboratories) by boiling for 5 minutes followed by cooling on ice. Equal amounts of protein sample were loaded and run on a 4-20% Mini-Protean TGX Polyacrylamide gel (Bio-Rad Laboratories). For αSMA and fibronectin, 25 μg of total protein was loaded. For TGF-β2, TGF-βR1, TSP-1, MMP3 and versican, 75 μg of total protein was loaded. After electrophoresis, proteins were transferred onto polyvinylidene difluoride membranes (Bio-Rad Laboratories) using a Bio-Rad Trans-Blot semi-dry system at 4°C. The membranes were blocked using 5% non-fat dry milk (Bio-Rad Laboratories) and then probed with antibodies overnight at 4°C against versican (Abcam: ab19345, polyclonal 1:500), MMP3 (Antibody Verify: AAS41420C, polyclonal 1:100), TSP-1 (Abcam: ab85762, polyclonal 1:500), TGFβ2 (Abcam: ab36495, monoclonal 1:500), TGFβR1 (Abcam: ab31013, polyclonal 1:500), αSMA (Sigma: A5228, monoclonal 1:500), or fibronectin (Abcam: ab2413, polyclonal 1:500). After incubation for 45 minutes with the secondary antibody tagged with horseradish peroxidase (anti-mouse or anti-rabbit, depending on the primary antibody used; Vector Labs), signal was visualized using an enhanced chemiluminescence detection system (Amersham Pharmacia Biotech, Cleveland, OH). Equal protein loading of protein lysates from TM from high- and low-flow regions was assessed by re-probing blots with an antibody against glyceraldehyde-3-phosphate dehydrogenase (GAPDH, Millipore [Burlington, MA]: MAB374, monoclonal 1:5000). Protein bands were imaged using ChemiDoc XRS+ imaging system (Bio-Rad Laboratories). Images were analyzed with ImageJ software (National Institutes of Health, Bethesda, MD). The images were inverted and bands manually segmented. Under the measure function, the band mean density and area were obtained. Their product was taken as the total band intensity. For each band, the background of the blot was determined the same way by sampling away from the lanes and subtracting from the total band intensity to yield a background corrected value. For each lane, the total band intensity of each experimental band was divided by the total band intensity of GAPDH from the same lane on the same blot to yield a GAPDH normalized densitometric value.

2.4. Microsphere Studies and Microscopy

In four of the donor eyes, confocal imaging was performed after application of ICG mixed with fluorescent microsphere (2 eyes), only ICG (1 eye), or only fluorescent microspheres (1 eye) (Supplemental Table 1). ICG aqueous angiographic images were taken at 5 min, and for

those eyes that received microspheres the eyes were prepared for microscopy after 1 hour. The fluorecent miscrospheres did not provide a bright enough signal for aqueous angiography, but standard ICG protocol did show signal. High- and low-flow regions were marked with a surgical pen as described above. All eyes were perfusion fixed as described above and wedges cut. The wedges were inverted, placed on a glass slide, and weighed down with a coverslip and a drop of phosphate-buffered saline. The tissues were then imaged with a Zeiss 710 NLO Laser Scanning Confocal Microscope (Cal Zeiss, Ag, Oberkochen, Germany) using a 2.5x Neofluar lens with an NA of 0.075. For ICG imaging, a 2P Chameleon laser was used (excitation 782 nm and emission at 600 nm). For imaging of the fluorescein isothiocyanate (FITC microspheres), an Argon laser was used (excitation 488 and emission at 500 to 550 nm). Images were collected (512 × 512 pixels and 16 –bit grayscale resolution) using Zeiss Zen software.

2.5. Statistical Analysis

For the analysis of the proteins by Western blot, the data obtained from the densitometric measurements were evaluated and expressed as normalized ratios to GAPDH. The experiments and analysis were performed in triplicate, each time using samples from a different donor eyes. The average integrated density was calculated with ± SEM and statistical analysis was performed evaluating three different samples with a Student's *t*-test with p-values <0.05 considered significant.

For immunofluorescent studies, fluorescence quantitative analyses was performed as described previously (Huang et al., 2016a; Huang et al., 2016b; Saraswathy et al., 2016). Briefly, average fluorescence pixel intensity was determined in a rectangular region of interest (57 × 95 pixels) centered on the TM area from both low- and high-flow sections (Adobe Photoshop CS5 v. 12×32; San Jose, CA) from which background signal in each slide (determined by sampling empty anterior chamber) was subtracted to obtain a background adjusted intensity. Statistical comparison of the background adjusted intensity values were conducted with unpaired two-sample Student's t-test. Relative fluorescence was quantitatively evaluated using six sections each from at least three different donors.

3. Results

3.1. Aqueous Angiography

Similar to our previously published reports, aqueous angiography in human enucleated eyes demonstrated segmental angiographic signal with high- and low-flow regions (Fig. 1; left column). Perfusing FITC-labeled beads mixed with ICG, regions of high- and low-flow were comparable (Fig. 1; middle column compared to left column). Two-photon microscopy was then performed for a more detailed evaluation of the TM AHO patterns (Fig 1A–I). A control eye receiving only fluorescent beads showed positive signal using the FITC microscopy settings but not the ICG microscopy settings (Fig. 1A–C). A control eye receiving only ICG showed positive signal using the ICG microscopy settings but not the FITC microscopy settings (Fig. 1D–F). When introduced into the eye as a mixture, co-localization of ICG and fluorescent beads was observed (Fig. 1G–I).

3.2. Aqueous Angiography and Known Segmental Targets

Previously, bead-based methods were used to isolate high- and low-flow TM showing a variety of alterations. A subset of those markers (versican, MMP3, and COLVI) were probed here based on aqueous angiography-determined high- and low-flow regions. From aqueous angiography-derived TM, Western blot showed relatively more versican (~2.9 ± 0.14-fold increase; p=0.003) in low-flow regions and relatively increased MMP3 (~2.2 ± 0.04-fold increase; p=0.01) in high-flow regions (Fig. 2). Immunofluorescence studies looking at the high- and low-flow areas of TM confirmed relatively higher levels of versican (~1.6 ± 0.1-fold; p=0.001) in the low-flow regions, whereas COLVI (~1.8 ± 0.4-fold; p=0.002) and MMP3 (~1.7 ± 0.2-fold; p=0.002) were expressed relatively more in high-flow regions (Fig. 3).

3.3. Aqueous Angiography and TGF-β Pathway Proteins

The TGF-β pathways are complex with multiple stimuli, ligands, and receptors. Here, using Western blot we demonstrated relative elevation of thrombospondin-1 (TSP-1) in low-flow regions (~2.7 ± 0.02-fold; p=0.001) (Fig. 4). TSP-1 is a known-upstream activator of TGF-β activity. Also, TGF-β2 ligand (~1.6 ± 0.02-fold; p=0.01) and TGF-β receptor 1 (~1.8 ± 0.03-fold; p=0.001) were relatively elevated in low-flow regions (Fig. 4).

3.4. Aqueous Angiography and TGF-β Downstream Targets

TGF-β signals through multiple pathways to impact multiple downstream targets. Among these include versican and COLVI (Verrecchia et al., 2001; Walton et al., 2017) which showed alterations above (Figs. 2 and 3). Other down-stream markers include αSMA which was found to be relatively elevated in TM low-flow regions by Western blot (~2.1 ± 0.08-fold; p=0.002) and immunofluorescence (~3.4 ± 1.2-fold; p=0.001) (Figs. 5 and 6). TGF-β can also specifically modulate ECM. In these experiments, while total fibronectin (FN) was not altered (IF: p=0.17, WB: p=0.31), relatively more FN-EDA (a FN isoform associated with fibrosis) was found in low-flow regions (~2.2 ± 0.3-fold; p=0.003) (Figs. 5 & 6).

4. Discussion

Segmental AHO was observed using both aqueous angiography and bead-based methods that were very similar to each other. Segmental biological differences were also found in aqueous angiography-derived low- and high-flow TM regions. These differences were consistent with prior research using bead-based methods for MMP3 and COLVI. Several additional differences were also observed. Specifically, relatively elevated TSP-1, TGF-β2, TGFβ–R1, and αSMA levels were seen in low-flow regions. Total FN was unchanged, but FN-EDA (a fibrosis-specific isoform of FN) was relatively increased in low-flow regions.

These results are consistent with a body of literature that has sought to understand the biology behind segmental flow and how this might be related to ocular hypertension in glaucoma. Previous studies have found increased TGF-β levels in the aqueous of glaucomatous patients (Agarwal et al., 2015). TGF-β is a known master regulator of fibrosis and can activate pro-fibrotic pathways that include αSMA, versican, and FN-EDA (Acott and Kelley, 2008; Baelde et al., 2004). Administration of TGF-β2 to the TM resulted in

further upregulation of TSP-1, implying a self-amplifying relationship (Wallace et al., 2014). Research has shown that TM was significantly thicker and less compacted in areas of high- compared to low-flow areas (Cha et al., 2016). Similarly, TM from glaucomatous eyes and low-flow regions of normal eyes showed increased stiffness (Vranka et al., 2018; Wang et al., 2018). Both of these findings could arise from increased TGF-β activity (Gabbiani, 2003; Walton et al., 2017; Wikner et al., 1988). Thus, the results of this investigation provide support for the TGF-β hypothesis where activation of pro-fibrotic pathways is associated with decreased AHO. In this study, the differences were specifically seen in low-flow TM regions of normal eyes. For glaucoma, increased IOP and outflow resistance may then come from an expansion of normal low-flow regions to shift the segmental TM (low-flow)/(high-flow) ratio higher.

Separately, the results of elevated versican in low-flow regions concurrent with increased MMP3 and COLVI in high-flow regions are interesting. Alterations in extracellular matrix have been implicated in outflow. For COLVI, elevated protein levels have been reported in both low-flow (at physiologic pressures) (Vranka et al., 2015) (Vranka and Acott, 2017) and high-flow (at elevated pressures) regions (Vranka et al., 2018). This implies biological response to pressure change. We note that the results in this paper were based on physiologic perfusion pressures such that the result of increased COLVI in low-flow regions is in agreement with the literature. For versican, increased outflow facility was further seen after perfusion of human or porcine anterior segment cultures with ADAMTS4, which cleaves versican (Keller et al., 2009). Versican silencing using RNAi mostly supported that result with increased outflow facility in porcine but unexpectedly decreased outflow facility in human anterior segment cultures (Keller et al., 2011). Increased MMP3 protein expression after AAV-mediated transduction of the corneal endothelium using *in vivo* mouse eyes was associated with increased outflow facility (O'Callaghan et al., 2017). Thus, increased MMP3 in aqueous angiography determined high-flow regions is also consistent with an enzymatic role to clear excessive material in the TM in order to promote AHO.

Further, it is important that there is agreement a) comparing segmental outflow patterns between aqueous angiography and bead-based methods and b) comparing segmental protein expression patterns in this paper (for COLVI, versican, and MMP3) with previous published data (Keller et al., 2011; Vranka et al., 2015). This agreement is interesting because bead-based methods directly visualize the TM and TM segmental flow (Keller et al., 2011; Vranka et al., 2015) while aqueous angiography instead visualizes AHO from an external perspective that highlights outflow distal to the TM. Aqueous angiographic signal is first observed at the intrascleral venous plexus and then flows to more downstream aqueous and episcleral veins. Thus, concordant results between aqueous angiography and bead-based outflow imaging methods show that the distal AHO pathway can be representative of TM AHO and physiology. This is important for clinicians since they can perform aqueous angiography but not bead-based labeling. Bead-based labeling safety has not been established, and its visualization occurs after cutting open the eye to expose the TM. In fact, this result was already hinted at during initial aqueous angiography research when trappable tracers were used and aqueous angiographically positive and negative regions were associated with and without TM tracer trapping, respectively (Huang et al., 2016a; Huang et

al., 2016b; Saraswathy et al., 2016). Together, all of these results further highlight the important role of the TM as a regulator of overall AHO.

The primary limitation of this study was that it utilized enucleated human eyes. Post-mortem artifacts related to cellular necrosis must be considered. Additionally, based on our aqueous angiography experience, post-mortem eyes do not show the entire gamut of AHO behaviors seen in living eyes such as dynamic AHO. AHO facility was also not measured here (although no attempts were made to manipulate it), and this can be included in the future. Further limitations exist with regard to how the tissues were processed. Protein isolation for Western blotting followed standard procedures. However, more specific fractionation for different tissue components (e.g. use of chaotropic agents for enrichment of extracellular proteins) could yield additional findings.

In conclusion, segmental biological differences were found using aqueous angiography derived low- and high-flow TM. Some of the observations were new while others supported findings obtained from previous and different methods. The overall results support the notion that TGF-β is associated with decreased AHO. The results also show that aqueous angiographic information is reflective of TM biology. Future work is needed to understand the relationship between segmental AHO and TGF-β in glaucomatous eyes. It may be that a pathological increase in the segmental TM low-flow/high-flow ratio is what leads to ocular hypertension in glaucoma. If this were the case, by understanding that process, it may be possible to prevent ocular hypertension before it occurs as opposed to ameliorating it after it arises.

Supplementary Material

Refer to Web version on PubMed Central for supplementary material.

Acknowledgements

Funding for this work came from National Institutes of Health, Bethesda, MD (Grant Numbers K08EY024674 [ASH]; R01EY030501 [ASH], R01EY029058 [RNW]; Research to Prevent Blindness Career Development Award 2016 [ASH]; and an unrestricted grant from Research to Prevent Blindness [UCLA and UCSD] (New York, NY). The funders had no role in study design, data collection and analysis, decision to publish, or preparation of the manuscript.

References

Abu-Hassan DW, Acott TS, Kelley MJ, 2014 The Trabecular Meshwork: A Basic Review of Form and Function. J Ocul Biol 2.

Acott TS, Kelley MJ, 2008 Extracellular matrix in the trabecular meshwork. Exp Eye Res 86, 543–561. [PubMed: 18313051]

Agarwal P, Daher AM, Agarwal R, 2015 Aqueous humor TGF-β2 levels in patients with open-angle glaucoma: A meta-analysis. Mol Vis 21, 612–620. [PubMed: 26019480]

Baelde HJ, Eikmans M, van Vliet AI, Bergijk EC, de Heer E, Bruijn JA, 2004 Alternatively spliced isoforms of fibronectin in immune-mediated glomerulosclerosis: the role of TGFbeta and IL-4. J Pathol 204, 248–257. [PubMed: 15372454]

Bentley MD, Hann CR, Fautsch MP, 2016 Anatomical Variation of Human Collector Channel Orifices. Invest Ophthalmol Vis Sci 57, 1153–1159. [PubMed: 26975026]

Braakman ST, Pedrigi RM, Read AT, Smith JA, Stamer WD, Ethier CR, Overby DR, 2014 Biomechanical strain as a trigger for pore formation in Schlemm's canal endothelial cells. Exp Eye Res 127, 224–235. [PubMed: 25128579]

Braakman ST, Read AT, Chan DW, Ethier CR, Overby DR, 2015 Colocalization of outflow segmentation and pores along the inner wall of Schlemm's canal. Exp Eye Res 130, 87–96. [PubMed: 25450060]

Brubaker RF, 2004 Goldmann's equation and clinical measures of aqueous dynamics. Exp Eye Res 78, 633–637. [PubMed: 15106943]

Camras LJ, Stamer WD, Epstein D, Gonzalez P, Yuan F, 2012 Differential effects of trabecular meshwork stiffness on outflow facility in normal human and porcine eyes. Invest Ophthalmol Vis Sci 53, 5242–5250. [PubMed: 22786899]

Carreon TA, Edwards G, Wang H, Bhattacharya SK, 2017 Segmental outflow of aqueous humor in mouse and human. Exp Eye Res 158, 59–66. [PubMed: 27498226]

Cha ED, Xu J, Gong L, Gong H, 2016 Variations in active outflow along the trabecular outflow pathway. Exp Eye Res 146, 354–360. [PubMed: 26775054]

Chang JY, Folz SJ, Laryea SN, Overby DR, 2014 Multi-scale analysis of segmental outflow patterns in human trabecular meshwork with changing intraocular pressure. J Ocul Pharmacol Ther 30, 213–223. [PubMed: 24456518]

Gabbiani G, 2003 The myofibroblast in wound healing and fibrocontractive diseases. J Pathol 200, 500–503. [PubMed: 12845617]

Gong H, Ruberti J, Overby D, Johnson M, Freddo TF, 2002 A new view of the human trabecular meshwork using quick-freeze, deep-etch electron microscopy. Exp Eye Res 75, 347–358. [PubMed: 12384097]

Hann CR, Bentley MD, Vercnocke A, Ritman EL, Fautsch MP, 2011 Imaging the aqueous humor outflow pathway in human eyes by three-dimensional micro-computed tomography (3D micro-CT). Exp Eye Res 92, 104–111. [PubMed: 21187085]

Huang AS, Belghith A, Dastiridou A, Chopra V, Zangwill LM, Weinreb RN, 2017a Automated circumferential construction of first-order aqueous humor outflow pathways using spectral-domain optical coherence tomography. J Biomed Opt 22, 66010. [PubMed: 28617922]

Huang AS, Camp A, Xu BY, Penteado RC, Weinreb RN, 2017b Aqueous Angiography: Aqueous Humor Outflow Imaging in Live Human Subjects. Ophthalmology 124, 1249–1251. [PubMed: 28461013]

Huang AS, Li M, Yang D, Wang H, Wang N, Weinreb RN, 2017c Aqueous Angiography in Living Nonhuman Primates Shows Segmental, Pulsatile, and Dynamic Angiographic Aqueous Humor Outflow. Ophthalmology 124, 793–803. [PubMed: 28237425]

Huang AS, Penteado RC, Papoyan V, Voskanyan L, Weinreb RN, 2019 Aqueous Angiographic Outflow Improvement after Trabecular Microbypass in Glaucoma Patients. Ophthalmol Glaucoma 2, 11–21. [PubMed: 31595267]

Huang AS, Penteado RC, Saha SK, Do JL, Ngai P, Hu Z, Weinreb RN, 2018 Fluorescein Aqueous Angiography in Live Normal Human Eyes. J Glaucoma 27, 957–964. [PubMed: 30095604]

Huang AS, Saraswathy S, Dastiridou A, Begian A, Legaspi H, Mohindroo C, Tan JC, Francis BA, Caprioli J, Hinton DR, Weinreb RN, 2016a Aqueous Angiography with Fluorescein and Indocyanine Green in Bovine Eyes. Transl Vis Sci Technol 5, 5.

Huang AS, Saraswathy S, Dastiridou A, Begian A, Mohindroo C, Tan JC, Francis BA, Hinton DR, Weinreb RN, 2016b Aqueous Angiography-Mediated Guidance of Trabecular Bypass Improves Angiographic Outflow in Human Enucleated Eyes. Invest Ophthalmol Vis Sci 57, 4558–4565. [PubMed: 27588614]

Johnson M, 2006 'What controls aqueous humour outflow resistance?'. Exp Eye Res 82, 545–557. [PubMed: 16386733]

Keller KE, Aga M, Bradley JM, Kelley MJ, Acott TS, 2009 Extracellular matrix turnover and outflow resistance. Exp Eye Res 88, 676–682. [PubMed: 19087875]

Keller KE, Bradley JM, Vranka JA, Acott TS, 2011 Segmental versican expression in the trabecular meshwork and involvement in outflow facility. Invest Ophthalmol Vis Sci 52, 5049–5057. [PubMed: 21596823]

Morrison JC, Cepurna Ying Guo WO, Johnson EC, 2011 Pathophysiology of human glaucomatous optic nerve damage: insights from rodent models of glaucoma. Exp Eye Res 93, 156–164. [PubMed: 20708000]

O'Callaghan J, Crosbie DE, Cassidy PS, Sherwood JM, Flugel-Koch C, Lutjen-Drecoll E, Humphries MM, Reina-Torres E, Wallace D, Kiang AS, Campbell M, Stamer WD, Overby DR, O'Brien C, Tam LCS, Humphries P, 2017 Therapeutic potential of AAV-mediated MMP-3 secretion from corneal endothelium in treating glaucoma. Hum Mol Genet 26, 1230–1246. [PubMed: 28158775]

Sabanay I, Gabelt BT, Tian B, Kaufman PL, Geiger B, 2000 H-7 effects on the structure and fluid conductance of monkey trabecular meshwork. Arch Ophthalmol 118, 955–962. [PubMed: 10900110]

Saraswathy S, Tan JC, Yu F, Francis BA, Hinton DR, Weinreb RN, Huang AS, 2016 Aqueous Angiography: Real-Time and Physiologic Aqueous Humor Outflow Imaging. PLoS One 11, e0147176. [PubMed: 26807586]

Snyder KC, Oikawa K, Williams J, Kiland JA, Gehrke S, Teixeira LBC, Huang AS, McLellan GJ, 2019 Imaging Distal Aqueous Outflow Pathways in a Spontaneous Model of Congenital Glaucoma. Transl Vis Sci Technol 8, 22.

Swaminathan SS, Oh DJ, Kang MH, Rhee DJ, 2014 Aqueous outflow: segmental and distal flow. J Cataract Refract Surg 40, 1263–1272. [PubMed: 25088623]

Tamm ER, 2009 The trabecular meshwork outflow pathways: structural and functional aspects. Exp Eye Res 88, 648–655. [PubMed: 19239914]

Verrecchia F, Chu ML, Mauviel A, 2001 Identification of novel TGF-beta /Smad gene targets in dermal fibroblasts using a combined cDNA microarray/promoter transactivation approach. J Biol Chem 276, 17058–17062. [PubMed: 11279127]

Vranka JA, Acott TS, 2017 Pressure-induced expression changes in segmental flow regions of the human trabecular meshwork. Exp Eye Res 158, 67–72. [PubMed: 27334250]

Vranka JA, Bradley JM, Yang YF, Keller KE, Acott TS, 2015 Mapping molecular differences and extracellular matrix gene expression in segmental outflow pathways of the human ocular trabecular meshwork. PLoS One 10, e0122483. [PubMed: 25826404]

Vranka JA, Staverosky JA, Reddy AP, Wilmarth PA, David LL, Acott TS, Russell P, Raghunathan VK, 2018 Biomechanical Rigidity and Quantitative Proteomics Analysis of Segmental Regions of the Trabecular Meshwork at Physiologic and Elevated Pressures. Invest Ophthalmol Vis Sci 59, 246–259. [PubMed: 29340639]

Wallace DM, Murphy-Ullrich JE, Downs JC, O'Brien CJ, 2014 The role of matricellular proteins in glaucoma. Matrix Biol 37, 174–182. [PubMed: 24727033]

Walton KL, Johnson KE, Harrison CA, 2017 Targeting TGF-beta Mediated SMAD Signaling for the Prevention of Fibrosis. Front Pharmacol 8, 461. [PubMed: 28769795]

Wang K, Li G, Read AT, Navarro I, Mitra AK, Stamer WD, Sulchek T, Ethier CR, 2018 The relationship between outflow resistance and trabecular meshwork stiffness in mice. Sci Rep 8, 5848. [PubMed: 29643342]

Weinreb RN, Khaw PT, 2004 Primary open-angle glaucoma. Lancet 363, 1711–1720. [PubMed: 15158634]

Wikner NE, Persichitte KA, Baskin JB, Nielsen LD, Clark RA, 1988 Transforming growth factor-beta stimulates the expression of fibronectin by human keratinocytes. J Invest Dermatol 91, 207–212. [PubMed: 2457630]

Highlights

Aqueous angiography is capable of visualizing segmental aqueous humor outflow (AHO) in living human eyes. Aqueous angiographic segmental AHO patterns matched that of bead-based methods which trap the tracer in the trabecular meshwork (TM). Aqueous angiographic determined high- and low-flow trabecular meshwork regions showed segmental changes in pro-fibrotic markers.

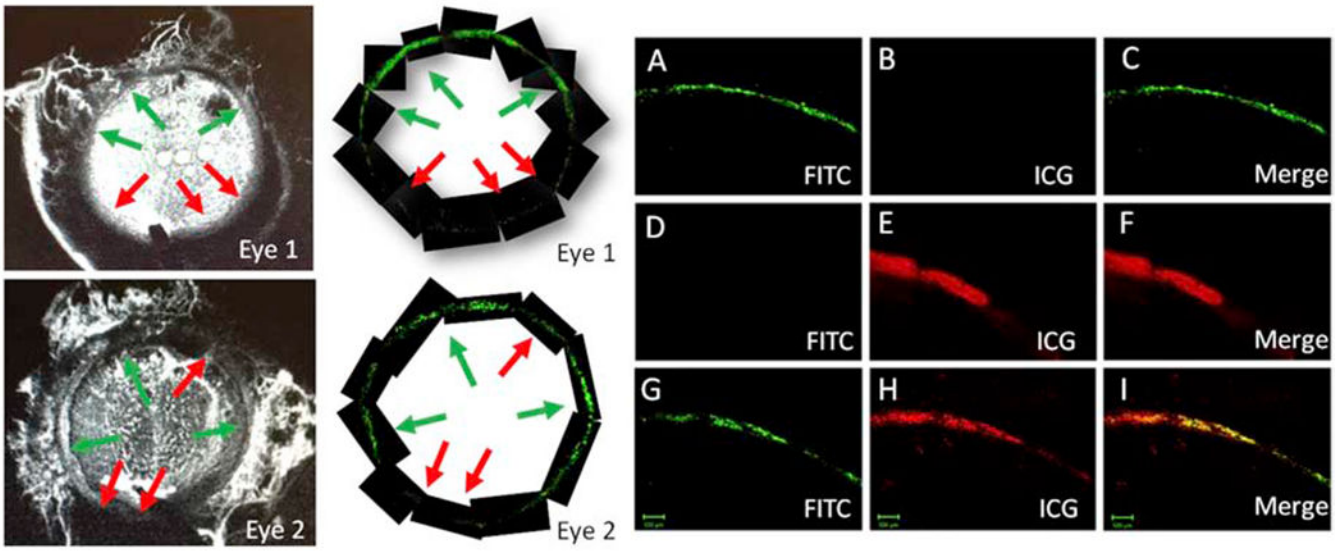

Figure 1. Aqueous Angiography with ICG and Fluorescent Beads in Post-Mortem Human Eyes.

Two eyes (Eyes 1 and 2) received fluorescent beads (FITC) diluted in ICG. Left Column: Indocyanine green (ICG) images taken at 5 min. Middle Column: Fluorescent bead imaging of the TM taken at 1 hour. High- and low-flow regions are denoted with green and red arrows, respectively. Note how the high- and low-flow regions match between the aqueous angiographic and bead-based methods. A-I) Then, using two-photon microscopy more detailed images of the TM were obtained. A-C) TM images from an eye that only received fluorescent beads. D-F) TM images from an eye that only received ICG. G-I) TM images from an eye (this is also Eye 1) that received both fluorescent beads and ICG.

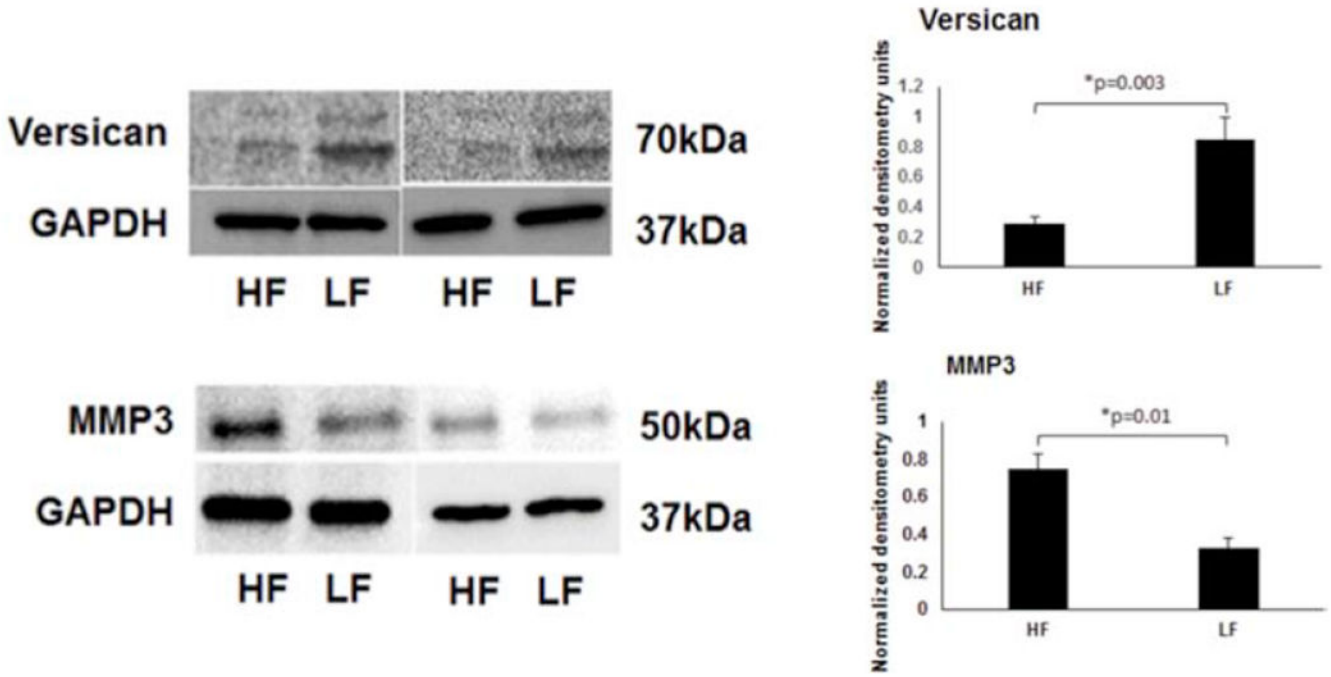

Figure 2. Differences in Versican and MMP3 Protein Expression in Segmental TM Outflow Regions by Western Blot.

Using bead-based segmental outflow assessment methods, prior research had demonstrated elevated versican in LF and MMP3 in HF regions (Keller et al., 2011; Vranka et al., 2015). Using aqueous angiography-determined TM tissue, elevated versican is also demonstrated in LF regions and MMP3 in HF regions. Sample size = 3 different eyes for each condition. Conditions compared by unpaired two-tailed Student's T-test and $p < 0.05$ was considered statistically significant. HF = high-flow and LF = low-flow. MMP3 = matrix metalloproteinase 3.

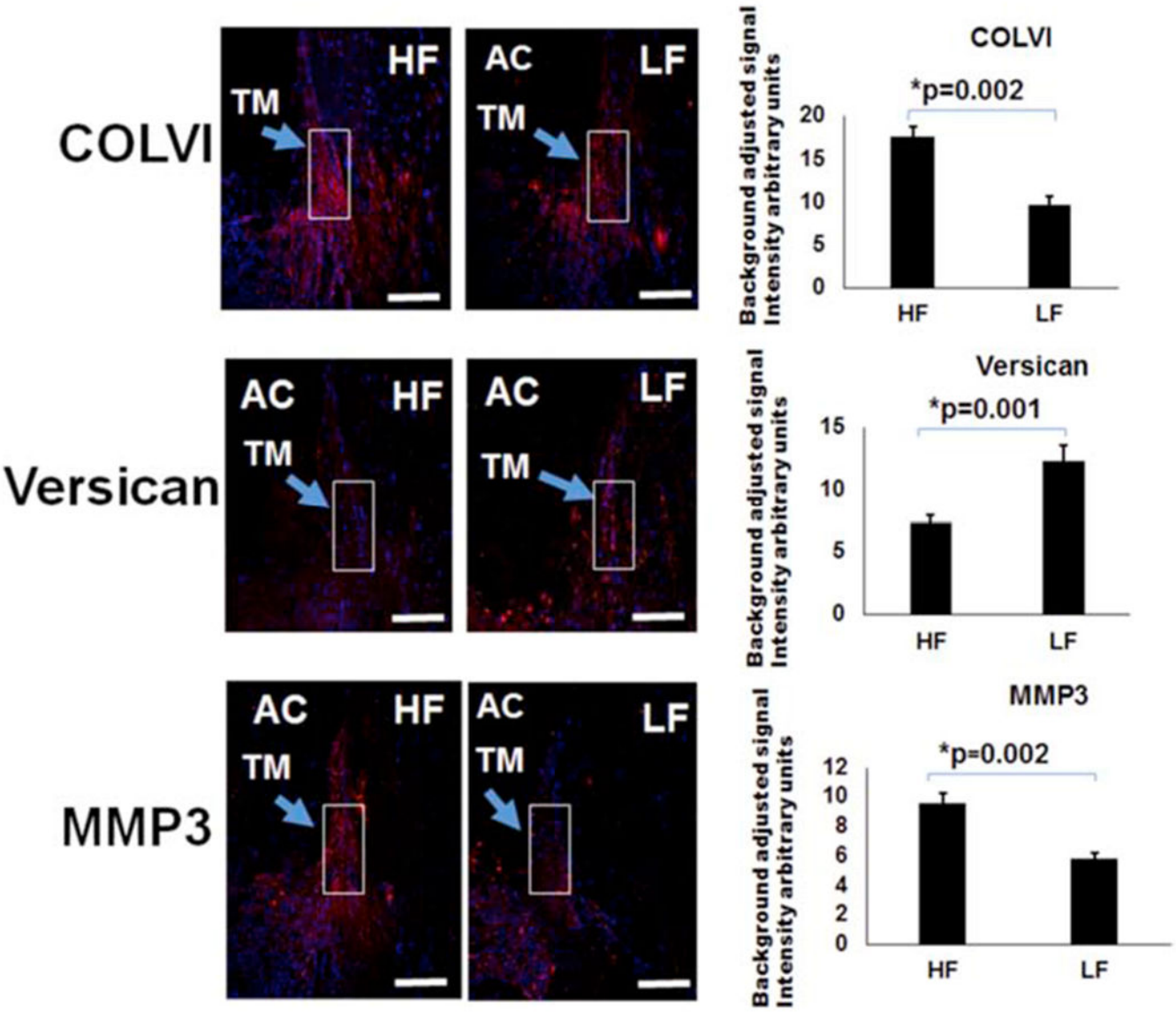

Figure 3. Differences in COLVI, Versican, and MMP3 in Segmental TM Outflow Regions by Immunofluorescence.

Immunofluorescence was performed for COLVI, versican, and MMP3. COLVI antibodies were unsuitable for Western blot. Using bead-based segmental outflow assessment methods, prior research had demonstrated elevated MMP3 and COLVI levels in HF regions and increased versican in LF regions (Keller et al., 2011; Vranka et al., 2015). Using aqueous angiography-determined angle sections, elevated COLVI was demonstrated in HF sections, versican in LF sections, and MMP3 in HF sections. White boxes demonstrate regions of interest that were used for quantification. Relative fluorescence was quantitatively evaluated using six sections each from at least three different donors and compared with an unpaired two-tailed Student's t-test. Scale bar = 100 microns. HF = high-flow and LF = low-flow. COLVI = collagen 6 and MMP3 = matrix metalloproteinase 3.

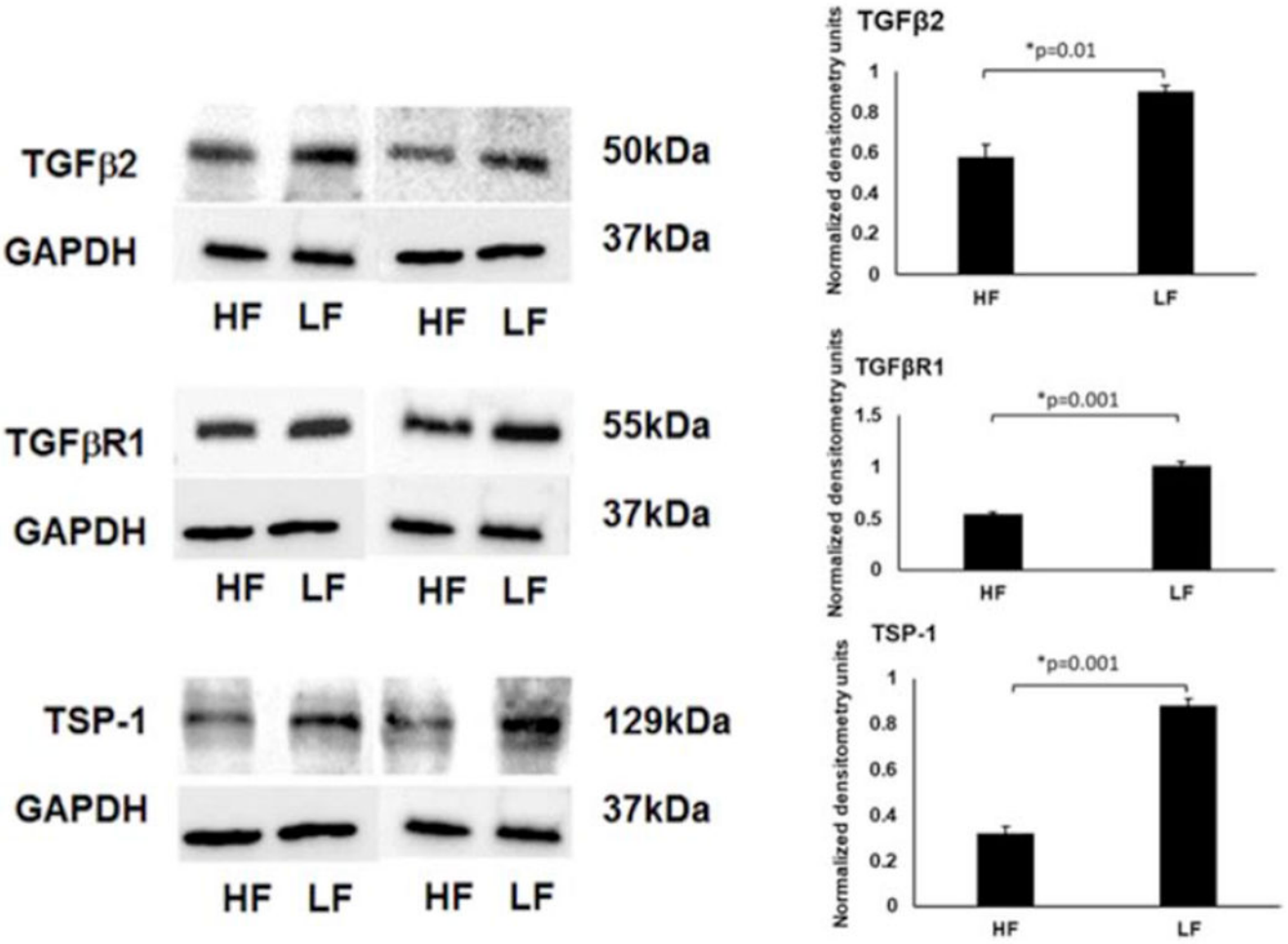

Figure 4. Differences in TSP-1, TGF-β2, and TGFβ-R1 Protein Expression in Segmental TM Outflow Regions by Western Blot.

Using aqueous angiography-determined TM tissue, elevated TSP-1, TGF-β2, and TGFβ–R1, were demonstrated in LF regions. Sample size = 3 different eyes for each condition. Conditions compared by unpaired two-tailed Student's T-test and $p < 0.05$ was considered statistically significant. HF = high-flow and LF = low-flow. TGFβ-2 = transforming growth factor beta-2, TGFβR1 = transforming growth factor beta receptor-1, and TSP-1 = thrombospondin-1.

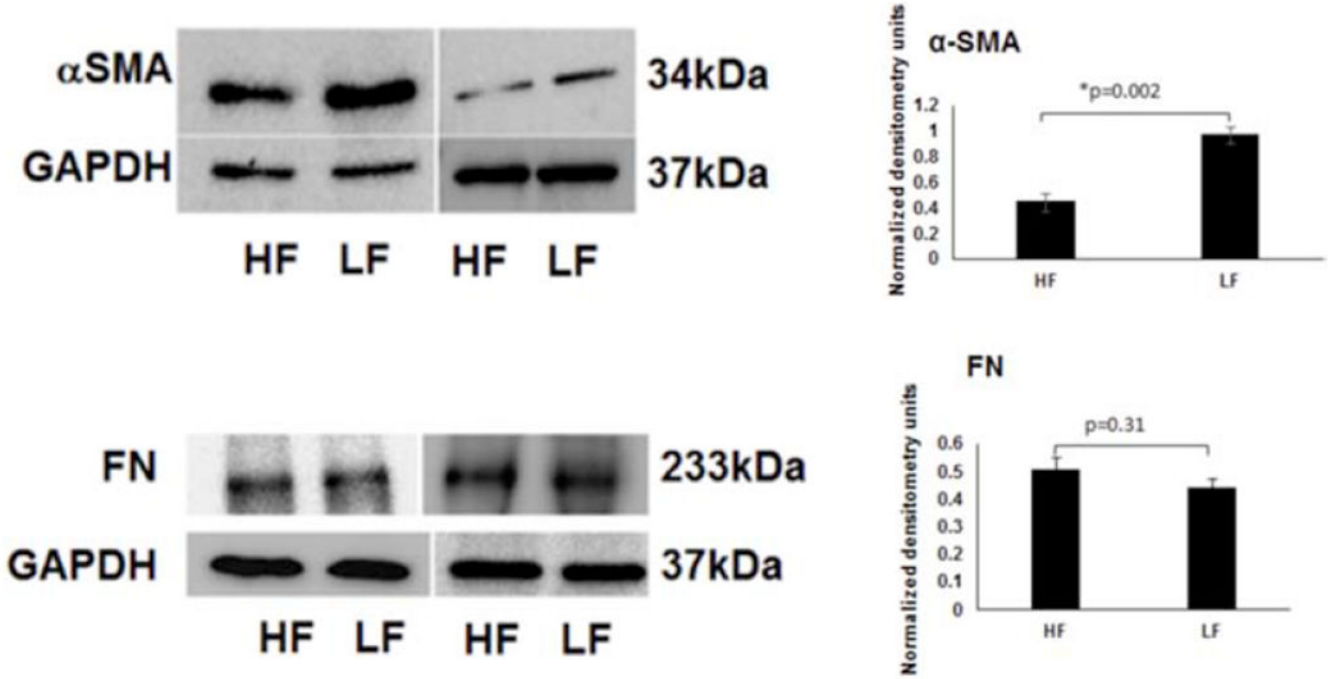

Figure 5. αSMA and Fibronectin (FN) Protein Expression in Segmental TM Outflow Regions by Western Blot.

Using aqueous angiography-determined TM tissue, elevated αSMA was demonstrated in LF regions. However, FN levels were not statistically significantly different comparing LF and HF regions. Sample size = 3 different eyes for each condition. Conditions compared by unpaired two-tailed Student's T-test and $p < 0.05$ was considered statistically significant. HF = high-flow and LF = low-flow. FN = fibronectin and αSMA = alpha-smooth muscle actin.

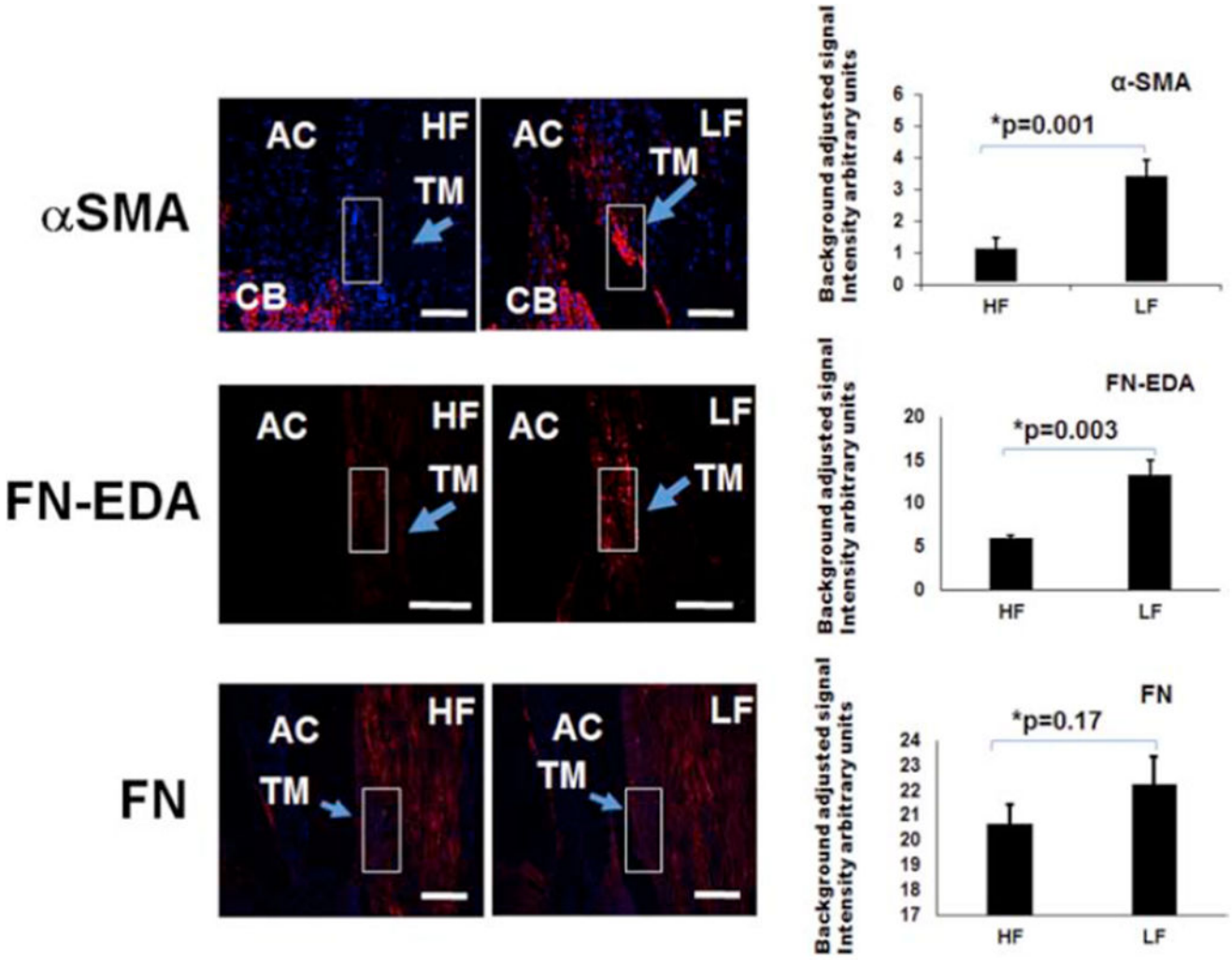

Figure 6. Differences in αSMA and, Fibronectin-EDA, and Fibronectin (FN) in Segmental TM Outflow Regions by Immunofluorescence.

Immunofluorescence was performed for αSMA, FN-EDA, and FN. FN-EDA antibodies were unsuitable for Western blot. Using aqueous angiography-determined angle sections, elevated αSMA and FN-EDA were demonstrated in LF sections. However, FN was not statistically significantly different comparing LF and HF sections. Relative fluorescence was quantitatively evaluated using six sections each from at least three different donors and compared with an unpaired two-tailed Student's t-test. Scale bar = 100 microns. HF = high-flow and LF = low-flow. αSMA = alpha-smooth muscle actin, FN-EDA = EDA isoform of fibronectin, and FN = fibronectin.